# Statistical Thermodynamics of Non-Stoichiometric Ceria and Ceria Zirconia Solid Solutions.

B. Bulfin,[*a] L. Hoffmann[a], L. de Oliveira[a], N. Knoblauch[b], F. Call[a], M. Roeb[a], C. Sattler[a], and M. Schmücker[b]

The thermodynamic redox properties of ceria and ceria zirconia solid solutions are analysed with a new methodology for modelling such systems based on the statistical mechanics of lattice configurations. Experimental thermogravimetric equilibrium data obtained for small non-stoichiometry measurements are combined with literature data to cover a large range of non-stoichiometry ($CeO_{2-\delta}$, $\delta = 0.001 - 0.32$), temperature (1073 - 1773 K) and oxygen partial pressure (1 - 10^{-13} bar). A dilute species model of defect clusters $(Ce'_{Ce}V_O^{\bullet\bullet}Ce'_{Ce})^{\times}$, obeying the law of mass action, was sufficient to describe the system over the whole range of conditions, leading to a simple analytical equation of state for the system. This offers new physical insight into the redox properties of ceria based materials, and the theoretical methods developed should also be of great interest for other materials which exhibit continuous oxygen non-stoichiometry similar to ceria, such as perovskite oxides.

Introduction

Cerium is the most abundant of the the rare earth elements, with a large annual production of approximately 24,000 mt.[1] Elemental cerium has the orbital structure $[Xe]4f^15d^16s^2$, making it the first element in the periodic table with an f orbital valence electron.[2] In metallic cerium, changes to this f orbital are responsible for the remarkable $\gamma - \alpha$ transition, where at a critical pressure the volume collapses by approximately 15 %, while preserving the fcc structure.[3] The ease at which the $4f$ state changes occupancy also plays an important role in the redox chemistry of ceria (CeO_2),[4] where oxygen vacancies are easily formed and can propagate through the planes of oxygen ions in the ceria fluorite phase. The net result is that ceria based oxides exhibit non-stoichiometry, the extent of which depends on the temperature and oxygen partial pressure[5,6].

$$CeO_2 \xleftrightarrow{\delta(T,p_{O_2})} CeO_{2-\delta} + \frac{\delta}{2}O_2, \qquad (1)$$
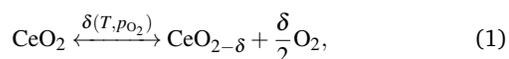
These remarkable redox properties combined with the relative abundance of ceria have lead to many applications as a redox catalyst including in auto-mobile catalytic converters and as a coating in self cleaning ovens.[7] It is also being investigated as a catalyst for the water gas shift,[8] steam reforming of hydrocarbons,[9] and as a co-catalyst in the Fischer-Tropsch process.[10] The high ionic conductivity of ceria based materials has lead to them being investigated as oxygen ion electrolytes for use in solid oxide fuel cells and electrolysis.[11,12] A solar powered thermochemical H_2O and CO_2 splitting cycle based on the ceria redox system has also been demonstrated,[13,14] which could offer a very attractive pathway to producing sustainable and environmentally benign liquid hydrocarbon fuels.[15]

In all of the above applications, a high concentration of oxygen vacancies is beneficial. The reducibility of ceria can be improved by substituting some of the cerium ions with zirconium ions.[6] The ionic radius of Ce^{3+} (1.14 Å) is much greater than that of Ce^{4+} (0.97 Å), resulting in a lattice expansion upon reduction.[16] The smaller ionic radius of Zr^{4+} (0.84 Å) compensates this expansion reducing the amount of strain induced in the lattice upon reduction, and thus improving the reducibility,[17] which also has been shown from first principle DFT studies.[18]

A full thermodynamic description requires both the enthalpy and entropy changes for the formation of oxygen vacancies to be determined. The latter can be very difficult due to the presence of both vibrational entropy changes in the lattice and the configuration entropy of introducing vacancies. The vibrational change in entropy can be well determined using DFT,[19] and Gopal *et al.* remarkably used a combination of ab initio DFT and cluster expansion Monte-Carlo simulations to model the overall trends of the configuration entropy.[20] On the other hand, experimentalists typically fit non-stoichiometry data by assuming that the defects in the ceria flourite structure have a dilute species behaviour.[5,21–25] In the case of pure ceria, this simple approach has not yet been enough to describe the data over a large range, with some authors suggesting that the type of defects and defect clusters change with

composition.[5,21,22]

In this work the problem of fitting equilibrium data with an analytical thermodynamic model is revisited. Experimental equilibrium data for oxygen vacancy concentration as a function of temperature and partial pressure is presented for both CeO_2 and $Ce_{0.85}Zr_{0.15}O_2$. A simple thermodynamic model is developed, using a dilute species statistical model for the entropy, and allowing the enthalpy to have a composition dependence. This model is then fit using the experimental data obtained here and additional equilibrium data from the literature. The model does not require any change in the type of defects or defect clusters. It has a simple analytical form making it an attractive tool for simulations as well as offering researches a simple method of modelling non-stoicheometry in ceria based materials.

Thermodynamic Model

It is assumed that there is a maximum reduction state that the reaction is proceeding towards, giving the complete reaction as

$$\frac{1}{\delta_m}CeO_2 \longrightarrow \frac{1}{\delta_m}CeO_{2-\delta_m} + \frac{1}{2}O_2, \tag{2}$$
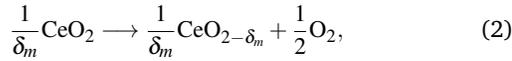
where δ_m is the maximum possible non-stoichiometry. In the literature it is common to fix this value to $\delta_m = 0.5$ in the case of CeO_2,[5,25] which corresponds to all of the cerium atoms switching from Ce^{4+} to Ce^{3+}. Here we assume that it could be less than this value and instead leave it as a free parameter that is fit using the experimental data.

Using Kröger-Vink notation for the defects, the unit-less vacancy concentration δ is defined as

$$\delta = \frac{\delta_m N_{V_O^{\bullet\bullet}}}{N_A}, \tag{3}$$

where the number of oxygen vacancies $N_{V_O^{\bullet\bullet}}$ is normalised with respect to the constant number of cerium atoms in equation 2, $N_{Ce} = \frac{1}{\delta_m}N_A$. Similarly the unit-less concentration of oxygen which can be removed from the lattice is given by

$$\delta_m - \delta = \frac{\delta_m N_{O_O^\times}}{N_A}, \tag{4}$$

where $N_{O_O^\times}$ only corresponds to the removable oxygen.

The equilibrium equations for the reduction reaction are,

$$\Delta g_\delta = \Delta g_\delta^\circ + \frac{1}{2}RT\ln\left(\frac{p_{O_2}}{p^\circ}\right) = 0, \tag{5}$$

$$\Delta g_\delta^\circ = \Delta h_\delta^\circ - T\Delta s_\delta^\circ. \tag{6}$$

where the δ subscript indicates they are partial molar quantities $\Delta g_\delta = \frac{\partial \Delta g}{\partial \delta}$, and the circular superscript indicates the value is at standard pressure. If the partial molar enthalpy change Δh_δ°, and entropy Δs_δ° are determined, then equations 5 and 6 give an equation of state.

Entropy

For the reaction given in equation 2, the change in entropy to produce δ oxygen vacancies starting from CeO_2 is given by

$$\Delta s_{vac}^\circ = \delta \Delta s_{th}^\circ + \Delta s_{con}. \tag{7}$$

The thermal entropy change Δs_{th}° is the entropy of oxygen gas plus the change in the lattice vibrational entropy caused by introducing vacancies

$$\Delta s_{th}^\circ = \frac{1}{2}s_{O_2}^\circ + \Delta s_v^\circ. \tag{8}$$

The entropy of oxygen gas depends on the temperature and in the range considered (1073-1773 K), $\frac{1}{2}s_{O_2}^\circ$ has a small variance of $128 \pm 4.5\,JK^{-1}\,mol^{-1}$,[26] but for simplicity it is assumed to be constant in the model.

The configuration entropy is determined by considering the statistical mechanics of lattice configurations, and in its most general form is given by

$$\Delta s_{con} = k_B \sum_{n=1}^{\Omega_{con}} P_n \ln(P_n), \tag{9}$$

where Ω_{con} is the number of configurations, with each configuration having a probability P_n. This is the number of distinct ways the oxygen ions $O_O^\times$, oxygen vacancies $V_O^{\bullet\bullet}$, cerium ions $Ce_{Ce}^\times$ and charged cerium ions Ce_{Ce}' can be arranged within the constraints of the lattice. In the work of Gopal et $al.$ they simulate many configurations of vacancies and cluster formations using DFT, and then using the ground state energies of these configurations together with a partition function the probabilities can be calculated.[20] Here we would like a simple analytical expression that can be fit to experimental data, so we make the dilute species assumption that all configurations have an equal probability reducing equation 9 to

$$\Delta s_{con} = k_B \ln(\Omega_{con}). \tag{10}$$

For $\delta > 0.01$ there is agreement in the literature that the defects are primarily doubly ionized oxygen vacancies.[5,21,22] The reduction reaction can then be written in Kröger-Vink notation as

$$O_O^\times + 2Ce_{Ce}^\times = V_O^{\bullet\bullet} + 2Ce_{Ce}' + \frac{1}{2}O_2, \tag{11}$$
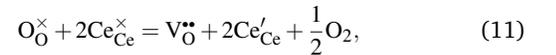
where the products can also form defect clusters of the form $(Ce_{Ce}'V_O^{\bullet\bullet}Ce_{Ce}')^\times$.

A formulae for the number of configurations is then given by

$$\Omega_{con} = \frac{(N_{V_O^{\bullet\bullet}} + N_{O_O^\times})!}{N_{V_O^{\bullet\bullet}}!N_{O_O^\times}!} + \frac{(N_{Ce_{Ce}'} + N_{Ce_{Ce}^\times})!}{N_{Ce_{Ce}'}!N_{Ce_{Ce}^\times}!}$$
$$+ N_{(Ce_{Ce}'V_O^{\bullet\bullet}Ce_{Ce}')}\,\omega_{(Ce_{Ce}'V_O^{\bullet\bullet}Ce_{Ce}')}, \tag{12}$$

where the first two terms are the standard configurations for the binary oxygen and cerium sub lattices respectively, and the last term accounts for the degrees of freedom of the defect clusters. This latter term assumes that each cluster has $\omega_{(Ce_{Ce}'V_O^{\bullet\bullet}Ce_{Ce}')}$ possible configurations (or micro-states). A useful simplification at

this point is to first count the configurations of the oxygen sub-lattice as a fully dilute species system, which for equation 2 gives the constraint

$$N_{V_O^{\bullet\bullet}} + N_{O_O^\times} = N_A. \qquad (13)$$

The effect of defect clusters can then be accounted for when counting the configurations of the cerium sub-lattice. For the cerium sub-lattice we have the general constraint

$$N_{Ce_{Ce}^\times} + N_{Ce_{Ce}'} + 2N_{(Ce_{Ce}'V_O^{\bullet\bullet}Ce_{Ce}')} = 2N_A \qquad (14)$$

Let's consider the two extreme cases of equation 12; all defects are randomly distributed with no defect clusters, and all defects form clusters of the form $(Ce_{Ce}'V_O^{\bullet\bullet}Ce_{Ce}')^\times$. This results in additional constraints for the two cases respectively

$$N_{Ce_{Ce}^\times} = 2N_{O_O^\times}, \; N_{Ce_{Ce}'} = 2N_{V_O^{\bullet\bullet}} \text{ and } N_{(Ce_{Ce}'V_O^{\bullet\bullet}Ce_{Ce}')} = 0, \qquad (15)$$

$$N_{(Ce_{Ce}'V_O^{\bullet\bullet}Ce_{Ce}')} = N_{V_O^{\bullet\bullet}} \text{ and } N_{Ce_{Ce}^\times} = N_{Ce_{Ce}'} = 0. \qquad (16)$$

Combining these constraints with equations 3, 4, 10 and 12, and applying Stirling's approximation leads to the configuration entropies

$$\Delta s_{con} = 3R(x\ln(x) + (1-x)\ln(1-x)), \qquad (17)$$

$$\Delta s_{con} = R(x\ln(x) + (1-x)\ln(1-x)) + xR\ln(\omega_{(Ce_{Ce}'V_O^{\bullet\bullet}Ce_{Ce}')}), \quad (18)$$

again for the two cases mentioned respectively, where the mole fraction $x = \frac{\delta}{\delta_m}$, and the first term in both equations is the standard entropy of mixing formulae.

A very good fit of the experimental data could be obtained using the second case given in equation 18 (see results section), which implies that most defects form $(Ce_{Ce}'V_O^{\bullet\bullet}Ce_{Ce}')^\times$ defect clusters. This is elaborated upon in the discussion section.

It should be noted here that the last term in equation 18 is a very simplified approach to accounting for the configurations of the defect clusters, but from the results it appears to be sufficient and physically meaningful.

Now, combining equation 7 and 18 gives

$$\Delta s_{vac} = \delta\Delta s_{th}^\circ + R(x\ln(x) + (1-x)\ln(1-x)), \qquad (19)$$

with

$$\Delta s_{th} = \frac{1}{2}s_{O_2}^\circ + \Delta s_v + \frac{1}{\delta_m}R\ln(\omega_{(Ce_{Ce}'V_O^{\bullet\bullet}Ce_{Ce}')}). \qquad (20)$$

Here the term $\frac{\delta}{\delta_m}R\ln(\omega_{(Ce_{Ce}'V_O^{\bullet\bullet}Ce_{Ce}')})$ from equation 18, has been combined into the thermal entropy as it is also linear in δ. This highlights the fact that the thermal and configuration entropy are often ambiguous, and this method is simply a means of interpretation.

From this interpretation, adding Zr^{4+} into the ceria lattice will block cerium lattice sites, thus reducing the degrees of freedom for the clusters. This term $\frac{\delta}{\delta_m}R\ln(\omega_{(Ce_{Ce}'V_O^{\bullet\bullet}Ce_{Ce}')})$, was included in the thermal entropy, and so the addition of Zr^{4+} is therefore expected to reduce the thermal entropy. This is discussed in more detail in the results section.

Finally in order to obtain the partial molar entropy we must take the derivative of equation 19 with respect to the vacancy concentration δ, giving

$$\Delta s_\delta^\circ(\delta) = \frac{\partial\Delta s_{vac}}{\partial\delta} = \Delta s_{th} + \frac{1}{\delta_m}R(\ln(\delta_m - \delta) - \ln(\delta)). \qquad (21)$$

Simple model

Combining equation 21 for the partial molar entropy with equations 5 and 6 gives the equation

$$\frac{1}{2}\ln\left(\frac{p_{O_2}}{p^\circ}\right) = \frac{-\Delta h_\delta^\circ}{RT} + \frac{\Delta s_{th}}{R} + \frac{1}{\delta_m}\ln\left(\frac{\delta_m - \delta}{\delta}\right) \qquad (22)$$

which can be re-arranged to give an equation of state

$$\left(\frac{\delta}{\delta_m - \delta}\right)^n = \left(\frac{p_{O_2}}{p^\circ}\right)^{-\frac{1}{2}}\exp\left(\frac{\Delta s_{th}}{R}\right)\exp\left(\frac{-\Delta h_\delta^\circ}{RT}\right). \qquad (23)$$

where $n = \frac{1}{\delta_m}$ if the law of mass action is obeyed. Mathematically this is similar to a previous equilibrium model developed from kinetic considerations.[27]

Corrected model

One issue with this model is that it requires a constant enthalpy of reaction. Experimental findings however show that the partial molar enthalpy varies with δ for both pure and Zr added ceria.[5,6,21,28]

In order to correct the simple model, the entropy dependence is assumed to be unchanged and the enthalpy dependence is added iteratively. The simple model (equation 23) is used to obtain a first approximation of vacancy concentration denoted δ', which is then used in the corrected model to determine Δh_δ°,

$$\left(\frac{\delta}{\delta_m - \delta}\right)^n = \left(\frac{p_{O_2}}{p^\circ}\right)^{-\frac{1}{2}}\exp\left(\frac{\Delta s_{th}}{R}\right)\exp\left(\frac{-\Delta h_\delta^\circ(\delta')}{RT}\right). \qquad (24)$$

The partial molar enthalpy is now $\Delta h_\delta^\circ(\delta')$. The dependence of the enthalpy on δ can be determined from experimental equilibrium data.

Experimental

Thermogravimetric analysis (TGA) was performed on samples of CeO_2 and $Ce_{0.85}Zr_{0.15}O_2$ in order to determine equilibrium vacancy concentrations $\delta(p_{O_2}, T)$. This experimental data can then be used, along with other literature sources to check the model.

To prepare the samples CeO_2 and $Ce_{0.85}Zr_{0.15}O_2$ powder were synthesized by Pechini method.[29] These powders were then kneaded with starch glue, dried and subsequently sintered at $1923\,K$ for $2\,h$, forming porous granules (4-5 mm diameter) for the TGA.

The samples were subject to XRD analysis to confirm that they were in the fluorite phase. The $Ce_{0.85}Zr_{0.15}O_2$ sample showed peak shifting which was consistent with Zr doped ceria.[30,31] In addition, EDX scans were also analysed to confirm the stoichiometry of the Zr doped sample. Sample characterization data and more details on the synthesis method are available in the ESI.

The thermogravimetric analyser (TGA) used in these experiments is a standard instrument offered by Netzsch (Model STA 449 F3 Jupiter). The concentration of oxygen in the TGA was controlled and measured using a combined pump and oxygen de-

tector produced by Nernst Setnag. The oxygen pump was used to set the partial pressure of oxygen in an argon stream before it entered the TGA and the sensor was used to measure the partial pressure of oxygen in the gas leaving the TGA. A schematic of the system is shown in the ESI.

The value of δ can be calculated from the mass changes measured in the TGA using the formula

$$\delta = \frac{\Delta m}{m} \frac{M_{\text{sample}}}{M_O}, \quad (25)$$

where m is the sample mass, M_O is the molar mass of molecular oxygen and M_{sample} is the molar mass of the sample.

Figure 1 shows typical data from a TGA experiment. The sample is first oxidised in synthetic air at 1173 K followed by heating to the desired reduction temperature under a low oxygen partial pressure argon stream. The partial pressure is then increased in steps and when the recorded mass values become constant, as indicated by the black arrow in fig. 1, the system is assumed to have reached equilibrium.
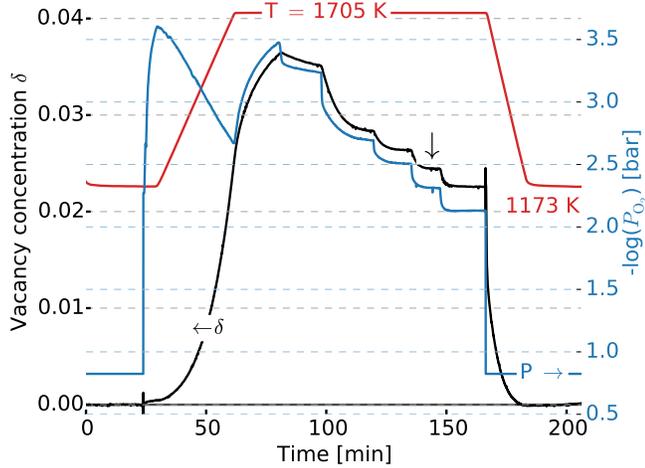

Fig. 1 Vacancy concentration δ, the oxygen partial pressure p_{O_2} and the temperature profile for a typical TGA experiment.

Results and Discussion

In order to fix the parameters of the corrected model we must first determine the dependence of the enthalpy on the vacancy concentration $\Delta h_\delta^\circ(\delta)$. To do this we use a combination of our experimental data and data from the literature.

For cerium dioxide there is a lot of thermodynamic data available in the literature.[5,21,23,32,33] In this work, the experimental data obtained here for small δ is presented as well as extracted data from the work of Panlener *et al.* and Takacs *et al.* .[5,21] For $Ce_{0.85}Zr_{0.15}O_2$, the experimental data obtained is presented along with the data of Hao *et al.* .[6]
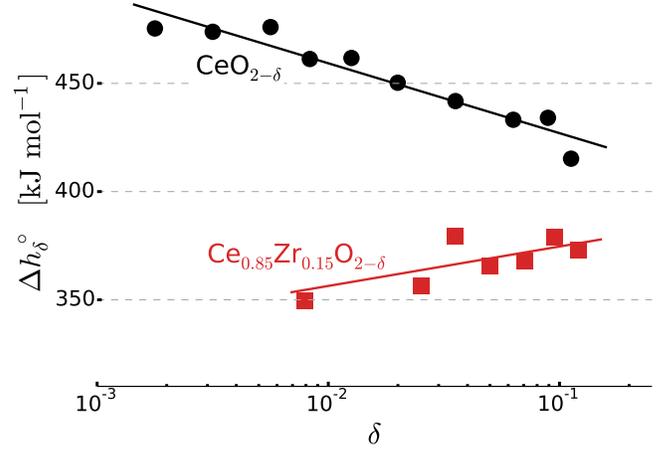

Fig. 2 Change in enthalpy for the reduction reaction vs. vacancy concentration δ. Also plotted are fits of the form $a + b\log(\delta)$ that are given in table 2.

0.1 Enthalpy

In order to determine the partial molar enthalpy for a given δ value one should note that equation 5 and 6 give the condition

$$\frac{1}{2}\ln\left(\frac{p_{O_2}}{p^\circ}\right) = \frac{-\Delta h_\delta^\circ}{RT} + \frac{\Delta s_\delta^\circ}{R}\bigg|_{\delta=const}. \quad (26)$$

Therefore, plots of $\frac{1}{2}\ln(p_{O_2})$ vs. $\frac{-1}{RT}$ for a given value of δ should give Δh_δ° as the slope.

To obtain the data at constant δ required for these plots, the experimental data and the literature data was interpolated between data points. None of the points were obtained by extrapolating, and each individual data set was interpolated separately. Figures illustrating this method are shown in the ESI.

Figure 2, shows the extracted enthalpy values for both CeO_2 and $Ce_{0.85}Zr_{0.15}O_2$, as well as fits of the data which are used in the corrected model for $\Delta h_\delta^\circ(\delta)$.

Model Fitting

The experimental equilibrium vacancy concentration values δ obtained in this work can be seen in figure 3. Note that the values of δ measured for CeO_2 were quite small, resulting in low mass changes and inevitably noisy data.

When fitting the data with the simple model (equation 23) the change in enthalpy is a constant, which was fixed by taking an average of literature values.[5,6,21] This model produces a better fit if the system is allowed to deviate from the law of mass action, $n \neq \frac{1}{\delta_m}$ (see table 1).

Table 1 Fit parameters of the simple model given in equation 23.

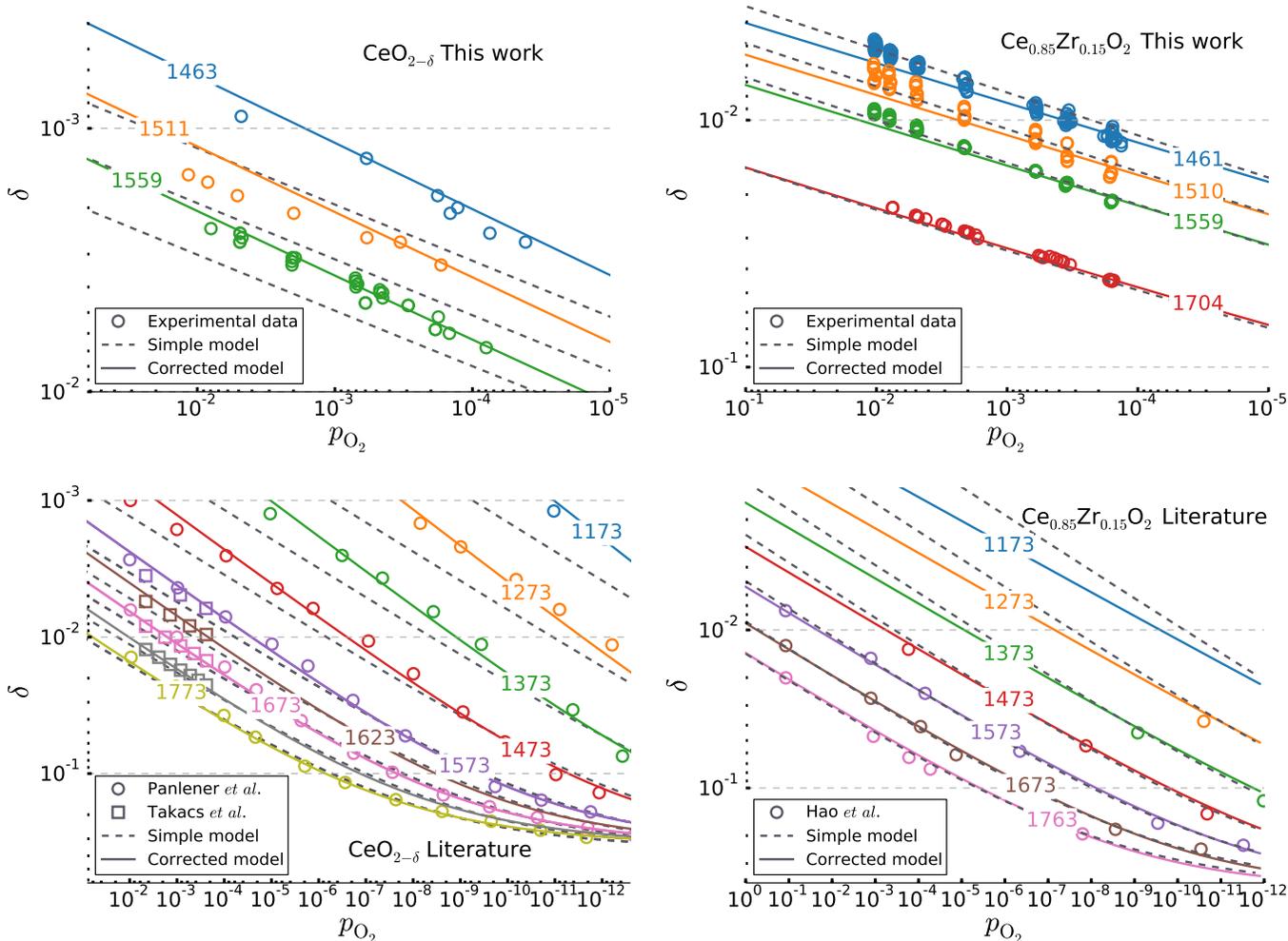|	Δh_δ° [kJ mol^{-1}]	δ_m [−]	n [−]	$\Delta s_{\text{th}}^\circ$ [JK^{-1}mol^{-1}]
CeO_2	430	0.35	2.31 ± 0.02	165 ± 5
$Ce_{0.95}Zr_{0.05}O_2$	395	0.41	2.44 ± 0.02	144 ± 6
$Ce_{0.85}Zr_{0.15}O_2$	370	0.425	2.81 ± 0.01	131 ± 5

Fig. 3 Experimental equilibrium δ values vs. p_{O_2}, recorded isothermally with in graph labels showing the temperature in Kelvin, for CeO_2 (left) and $Ce_{0.85}Zr_{0.15}O_2$ (right) plotted with the best fit for both the simple model (equation 23) and the corrected model (equation 24). **Above**: Data from this work. **Below:** Data from the literature.[5,6,21]

However, the corrected model (equation 24), which includes the enthalpy changing with composition, provides a better fit and also obeys the law of mass action, $n = \dfrac{1}{\delta_m}$. This shows that the system is well modelled as a dilute mixture of $(Ce'_{Ce}V^{\bullet\bullet}_{O}Ce'_{Ce})^{\times}$ defect clusters with an enthalpy of reaction that depends on the composition.

For very low vacancy concentrations in $CeO_{2-\delta}$ ($\delta \to 0$), the formation of defect clusters is less likely, and thus the model will underestimate the configuration entropy change and thus also δ. This can be seen in figure 3 for values of δ close to 0.001.

Figure 3 also shows the experimental data for $Ce_{0.85}Zr_{0.15}O_2$ as well as data from Hao *et al.* .[6] Again it can be seen that the corrected model offers a better fit of the data, and obeyed the law of mass action. The parameters of both the simple and corrected model can be seen in tables 1 and 2 respectively.

$Ce_{0.95}Zr_{0.05}O_2$ was also fit with the simple model (see ESI) using data from Takacs *et al.* and Hao *et al.* .[6,21] Interestingly, the simple model in this case obeyed the law of mass action and offered a reasonably good fit. This makes sense as the partial

Table 2 Fit parameters of the corrected model given in equation 24. The fit values of Δh°_δ are plotted in figure 2.

	Δh°_δ [kJ mol^{-1}]	$n = \dfrac{1}{\delta_m}$ [−]	Δs°_{th} [J K^{-1} mol^{-1}]
CeO_2	$395 - 31.4\log(\delta)$	2.90 ± 0.01	160 ± 5
$Ce_{0.85}Zr_{0.15}O_2$	$392 + 18.22\log(\delta)$	2.353 ± 0.01	137.5 ± 2

molar enthalpy for this material is approximately constant and thus the simple model should adequately describe the system.

One of the main differences in the fits of the materials is the value of Δs°_{th}, which decreases with increasing Zr concentration. This makes good physical sense, as the thermal entropy here includes the term $\dfrac{1}{\delta_m}R\ln(\omega_{(Ce'_{Ce}V^{\bullet\bullet}_{O}Ce'_{Ce})})$, which corresponds to the degrees of freedom of the defect clusters. For the Zr added samples, the fit values of δ_m increased, and $\omega_{(Ce'_{Ce}V^{\bullet\bullet}_{O}Ce'_{Ce})}$ should decrease, as Zr^{4+} ions will reduce the number of lattice cites that Ce'_{Ce} defects can occupy.

From the values given in table 2, a simple estimate for the

difference expected in $\Delta s_{\text{th}}^{\circ}$ between CeO_2 and $Ce_{0.85}Zr_{0.15}O_2$ is $R(2.9\ln(10) - 2.344\ln(8.5)) \approx 14\,JK^{-1}\,mol^{-1}$. This is relatively close to that obtained from the model fits of $\approx 22\,JK^{-1}\,mol^{-1}$, especially considering the crude estimate used for the effect Zr^{4+} would have on $\omega_{(Ce'_{Ce}V_O^{\bullet\bullet}Ce'_{Ce})}$.

Discussion

The major differences between the model used here and those used in previous studies are; the inclusion of the enthalpy's composition dependence, and the maximum stoicheometry change δ_m was not fixed and instead was fit using the data. It is more usual to assume that all of the cerium ions can be in the Ce^{3+} state, which gives the values $\delta_m = 0.5, 0.475$ and 0.425 for CeO_2, $Ce_{0.95}Zr_{0.05}O_2$ and $Ce_{0.85}Zr_{0.15}O_2$ respectively.

Taking these fixed values of δ_m, an interesting alternative model can be obtained by assuming that there could be some mixture of free defects and defect clusters giving a weighted average of equations 17 and 18,

$$\Delta s_{\text{vac}}^{\circ} = \delta\Delta s_{\text{th}}^{\circ} + aR(x\ln(x) + (1-x)\ln(1-x)), \quad (27)$$

where

$$\Delta s_{\text{th}}^{\circ} = \frac{1}{2}s_{O_2}^{\circ} + \Delta s_v^{\circ} + \frac{1}{\delta_m}R\ln(\omega_{\text{clusters}}), \quad (28)$$

$$1 \leq a \leq 3. \quad (29)$$

The value of a is then a measure of the extent of cluster formations, where $a = 3$ implies no defect clusters are present and $a = 1$ corresponds to all defects forming $(Ce'_{Ce}V_O^{\bullet\bullet}Ce'_{Ce})^{\times}$ clusters. Intuitively, one would also expect this model to offer information about more complicated arrangements. For example if there are interactions between defect clusters leading to energetically preferential arrangements or some semi ordered phases, then one would expect the value of a to be less than 1.

Differentiating equation 27 gives

$$\Delta s_{\delta}^{\circ}(\delta) = \frac{\partial \Delta s_{\text{vac}}^{\circ}}{\partial \delta} = \Delta s_{\text{th}}^{\circ} + \frac{a}{\delta_m}R(\ln(\delta_m - \delta) - \ln(\delta)). \quad (30)$$

This model was also used to fit the data with the parameter a left free and δ_m fixed at the maximum values given above. Again the enthalpy dependence was also included.

Figure 4 shows the entropy data and the two different models proposed. In the case of $Ce_{0.85}Zr_{0.15}O_2$ both models are essentially identical as the fit δ_m was already very close to the maximum value of 0.425, and $a \approx 1$ for the alternative model. For pure CeO_2 the differences are more pronounced. For the alternative model (equation 30) the value of a from this fit was 1.83 suggesting that there is some mixture of free defects and defect clusters, which has been suggested by other authors in the literature.[5,21] For small δ the alternative model deviates more from the experimental $\Delta s_{\delta}^{\circ}$ values from this work and the literature. The models predicted δ values are very sensitive to the entropy dependence and so the alternative model does not offer a good fit to the experimental δ values, especially for $\delta < 0.2$ (plots in ESI).

In the literature other authors have approached this by as-
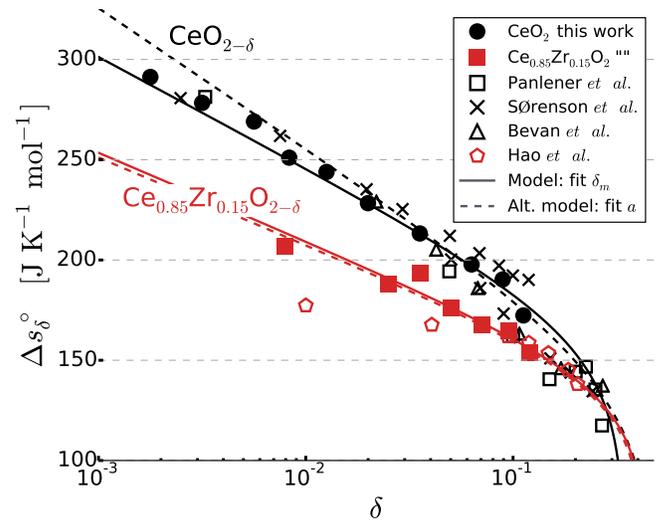

Fig. 4 The partial molar entropy $\Delta s_{\delta}^{\circ}$ vs. δ, extracted from the same data as $\Delta h_{\delta}^{\circ}$, plotted along with literature data, the δ_m fit model (equation 21) and the alternative a fit model (equation 30).

suming that the dominant defect behaviour changes with δ,[22,34] which would correspond to giving a a dependence on δ. The physical reasoning behind this could be due to the change in unit-cell volume changing the interactions between defects. Introducing an additional dependence $a(\delta)$, can indeed lead to a good fit over the data range, but it greatly increases the complexity of the model and the fitting process.

Experimental data for CeO_2 indirectly supports the initial model given in equation 24 with $\delta_m = 0.345$, in that no value greater than this has been experimentally measured. For pure ceria in the fluorite phase, the largest value of δ in the literature is 0.33, which was measured by Ban and Nowick for a single crystal of CeO_2.[35] Their attempts to reach a higher reduction state resulted in decomposition to Ce_2O_3. In addition, the change in $\Delta s_{\text{th}}^{\circ}$ as a result of substituting in Zr^{4+} was predictable. This was not the case in the alternative a model (equation 30), in which $\Delta s_{\text{th}}^{\circ}$ was found to be independent of Zr^{4+} concentration. The maximum vacancy concentration $\delta_m = 0.345$ could mean that there is something limiting the number of possible oxygen vacancies other than all Ce^{4+} being converted to Ce^{3+}. For example the reduction could be proceeding towards some defect ordered structure at $\delta \approx 0.345$, with further reduction requiring a full phase change to Ce_2O_3.

Conclusions

Overall, this work offers a new physical understanding of ceria based redox materials. The redox thermodynamics of all three materials investigated (CeO_2, $Ce_{0.95}Zr_{0.05}O_2$ and $Ce_{0.85}Zr_{0.15}O_2$) can be appropriately described by a statistical dilute species model of defect clusters $(Ce'_{Ce}V_O^{\bullet\bullet}Ce'_{Ce})^{\times}$, where in the case of ceria the maximum non-stoichiometry was limited to $\delta_m = 0.345$. The model was improved by giving the partial molar enthalpy of reaction a compositional dependence, which was determined using experimental equilibrium data from this work and the literature. Addition of Zr^{4+} into the ceria lattice decreases both the change in en-

thalpy and entropy of the reduction reaction. The decrease in the change in entropy can now be understood as Zr^{4+} ions blocking lattice sites in the cerium sub-lattice and thus reducing it's associated configuration entropy. The methodology used here should also apply to many perovskites, which show very similar redox behaviour to the ceria system[36].

Acknowledgements

Electronic Supplementary Information

The ESI contains more detailed sample production information, sample characterisation data, a schematic of the experimental system, some additional model fitting graphs for $Ce_{0.95}Zr_{0.05}O_2$, and the fit of an alternative model to the CeO_2 data.

References

1 C. Hammond and D. Lide, *CRC handbook of chemistry and physics*, 2005, 45–97.

2 W. C. Martin, L. Hagan, J. Reader and J. Sugar, *J. Phys. Chem. Ref. Data*, 1974, **3**, 771–780.

3 J. Allen and R. M. Martin, *Phys. Rev. Lett.*, 1982, **49**, 1106.

4 N. Skorodumova, S. Simak, B. I. Lundqvist, I. Abrikosov and B. Johansson, *Phys. Rev. Lett.*, 2002, **89**, 166601.

5 R. Panlener, R. Blumenthal and J. Garnier, *J. Phys. Chem. Solids*, 1975, **36**, 1213–1222.

6 Y. Hao, C.-K. Yang and S. M. Haile, *Chem. Mater.*, 2014, **26**, 6073–6082.

7 A. Trovarelli, C. de Leitenburg, M. Boaro and G. Dolcetti, *Catal. Today*, 1999, **50**, 353–367.

8 T. Bunluesin, R. Gorte and G. Graham, *Appl. Catal., B*, 1998, **15**, 107–114.

9 B. Zhang, X. Tang, Y. Li, Y. Xu and W. Shen, *Int. J. Hydrogen Energy*, 2007, **32**, 2367–2373.

10 L. Spadaro, F. Arena, M. Granados, M. Ojeda, J. Fierro and F. Frusteri, *J. Catal.*, 2005, **234**, 451–462.

11 V. Kharton, F. Figueiredo, L. Navarro, E. Naumovich, A. Kovalevsky, A. Yaremchenko, A. Viskup, A. Carneiro, F. Marques and J. Frade, *J. Mater. Sci.*, 2001, **36**, 1105–1117.

12 B. Zhu, I. Albinsson, C. Andersson, K. Borsand, M. Nilsson and B.-E. Mellander, *Electrochem. Commun.*, 2006, **8**, 495–498.

13 P. Furler, J. R. Scheffe and A. Steinfeld, *Energy Environ. Sci.*, 2012, **5**, 6098–6103.

14 W. C. Chueh, C. Falter, M. Abbott, D. Scipio, P. Furler, S. M. Haile and A. Steinfeld, *Science*, 2010, **330**, 1797–1801.

15 D. Marxer, P. Furler, J. Scheffe, H. Geerlings, C. Falter, V. Batteiger, A. Sizmann and A. Steinfeld, *Energy Fuels*, 2015, **29**, 3241–3250.

16 H.-W. Chiang, R. N. Blumenthal and R. A. Fournelle, *Solid State Ionics*, 1993, **66**, 85–95.

17 A. Bonk, A. Remhof, A. C. Maier, M. Trottmann, M. V. Schlupp, C. Battaglia and U. F. Vogt, *J. Phys. Chem. C*, 2015.

18 H.-F. Wang, X.-Q. Gong, Y.-L. Guo, Y. Guo, G. Z. Lu and P. Hu, *J. Phys. Chem. C*, 2009, **113**, 10229–10232.

19 S. Grieshammer, T. Zacherle and M. Martin, *Phys. Chem. Chem. Phys.*, 2013, **15**, 15935–15942.

20 C. B. Gopal and A. van de Walle, *Phys. Rev. B*, 2012, **86**, 134117.

21 M. Takacs, J. Scheffe and A. Steinfeld, *Phys. Chem. Chem. Phys.*, 2015, **17**, 7813–7822.

22 H. Tuller and A. Nowick, *J. Electrochem. Soc.*, 1979, **126**, 209–217.

23 O. T. Sørensen, *J. Solid State Chem.*, 1976, **18**, 217–233.

24 M. Zinkevich, D. Djurovic and F. Aldinger, *Solid State Ionics*, 2006, **177**, 989–1001.

25 J. Campserveux and P. Gerdanian, *Journal of Solid State Chemistry*, 1978, **23**, 73–92.

26 P. J. Linstrom and W. Mallard, 2001.

27 B. Bulfin, A. J. Lowe, K. A. Keogh, B. E. Murphy, O. Lubben, S. A. Krasnikov and I. V. Shvets, *J. Phys. Chem. C*, 2013, **117**, 24129–24137.

28 M. Kuhn, S. Bishop, J. Rupp and H. Tuller, *Acta Mater.*, 2013, **61**, 4277–4288.

29 M. Pechini, *US Patent, 3.330. 697*, 1967.

30 B. Bulfin, F. Call, J. Vieten, M. Roeb, C. Sattler and I. Shvets, *J. Phys. Chem. C*, 2016.

31 F. Call, M. Roeb, M. Schmücker, C. Sattler and R. Pitz-Paal, *J. Phys. Chem. C*, 2015, **119**, 6929–6938.

32 D. Bevan and J. Kordis, *J. Inorg. Nucl. Chem.*, 1964, **26**, 1509–1523.

33 P. Campserveux, J; Gerdanian, *J. Solid State Chem.*, 1978.

34 S. Bishop, K. Duncan and E. Wachsman, *Electrochim. Acta*, 2009, **54**, 1436–1443.

35 Y. Ban and A. S. Nowick, Proceeding of the 5th Materials research symposium, 1972, p. 353.

36 E. Bakken, T. Norby and S. Stølen, *J. Mater. Chem.*, 2002, **12**, 317–323.